DISCLAIMER

This draft chapter is a work in progress and is being provided to the public for information purposes only. Because it is a work in progress, there are parts that are either missing or will be revised, and the page numbers will change. Permission to cite any part of this work must be obtained from the prime author. The final version of this chapter will be published in Volume 9 of the *SeaWiFS Postlaunch Technical Report Series*.

Chapter 3

Lunar Data Analysis for SeaWiFS Calibration

Robert E. Eplee, Jr., and Robert A. Barnes
SAIC General Sciences Corporation, Beltsville, Maryland

Abstract

The SeaWiFS CVT uses monthly lunar calibrations to monitor long-term stability of the radiometric calibration of SeaWiFS. The procedures and results of this analysis are described in this chapter.

3.1 INTRODUCTION

The SeaWiFS Calibration and Validation program uses on-orbit calibration data to monitor the radiometric stability of the SeaWiFS bands over the course of the mission. The CVT of the SeaWiFS Project uses monthly lunar calibrations to track the long-term stability of the radiometric calibration of SeaWiFS. The time series of lunar calibrations are used to compute any time correction factors required to maintain a stable radiometric sensitivity for each of the SeaWiFS bands over the course of the mission. The lunar data analysis techniques and preliminary results were previously discussed by Barnes et al. (1998 and 1999) and by Barnes and McClain (1999). This chapter describes how these techniques are used to generate the time corrections for the SeaWiFS calibration table.

The time correction factors are defined in the SeaWiFS level-1b calibration equation (discussed in detail in Johnson et al. 1999):

$$\begin{aligned} L_S(\lambda) \; = & \left(C_{\text{out}}(\lambda) \; - \; C_{\text{dark}}(\lambda)\right) K_1(g,d,\lambda) \\ & \times \left(1 + K_2(\lambda)\,(T \; - \; T_{\text{ref}})\right) K_3(\text{pxl},\lambda) \\ & \times \; M(\text{ms},\lambda)\,\alpha(\lambda)\left(\beta(\lambda) \; + \; \gamma(\lambda)\,(t \; - \; t_o)\right. \\ & + \; \left.\delta(\lambda)\,(t \; - \; t_o)^2\right) \end{aligned}, \quad (1)$$

where:

- λ is the wavelength of measurement;
- L_S is the calibrated at-sensor radiance;
- C_{out} is the counts from sensor output data;
- C_{dark} is the dark count from sensor output data;
- K_1 is the counts to radiance conversion factor (calibration coefficient);
- g is the gain;
- d is the detector;
- K_2 is the detector temperature-dependent correction factor;
- T is the detector temperature from sensor output data;
- T_{ref} is the reference temperature (20°C);
- K_3 is the scan modulation correction;
- pxl is the pixel number along scan line;
- M is the half-angle mirror side correction factor;
- ms is the mirror side (a or b);
- α is the vicarious gain;
- β is the constant term in temporal correction;
- γ is the linear (in time) term in temporal correction;
- δ is the quadratic (in time) term in temporal correction;
- t is the time tag of sensor output data; and
- t_o is the reference time for temporal correction.

The reference time for the temporal correction is the time tag of the first SeaWiFS on-orbit image, which was obtained on 4 September 1997 at 16:26:30 UT. The current design of the SeaWiFS level-1b algorithm allows for a multisegment quadratic time correction.

3.2 LUNAR CALIBRATIONS

Lunar calibrations are performed once per month when the moon is at a phase angle (θ) of approximately 7°. This phase angle is chosen to maximize the illuminated surface of the moon while minimizing the opposition effect, the surge in brightness of sunlight diffusely reflected from a particulate surface near zero phase. Operational considerations, such as a conflict of the lunar measurement with a midnight data downlink, will require that the measurements be moved on occasion to different phase angles or from before full phase to after full phase.

SeaWiFS operates in a sun-synchronous orbit, crossing the equator from north to south at local noon. In normal operation, the spacecraft is maintained in a nadir orientation, using pitch-axis momentum wheels for attitude control, with a spacecraft pitch rate of 360° per orbit

(about 0.06° per second). For lunar measurements, the rotation rate of the momentum wheels is increased and the spacecraft is pitched in the opposite direction at a rate of approximately 0.15° per second. The maneuver is started after the spacecraft crosses the South Pole and is timed so that SeaWiFS will view the moon as the spacecraft ground track crosses the sublunar point. At the end of the maneuver, when the spacecraft again points toward the Earth, the pitch rate is returned to normal. During the maneuver, SeaWiFS is oriented so that it scans across the lunar surface from west to east in celestial coordinates.

Because the moon appears to be a stationary object during the SeaWiFS measurements, the number of scan lines in lunar calibration depends on the pitch rate of the instrument and the apparent size of the moon. The pitch rate causes SeaWiFS to oversample the moon, resulting in approximately 26 scan lines of the moon in a typical lunar image that has a diameter of approximately 7 pixels.

For the calibration data analysis, disk-integrated spectral radiances are computed for each band from the lunar images. Prelaunch modeling of simulated lunar images showed that disk-integrated spectral radiances produce more consistent results than those computed for one or a few pixels from the center of the lunar image (Woodward et al. 1993). In this analysis, the disk-integrated radiances are summed over all pixels in the lunar image whose brightness is greater than 1% of the peak brightness in the image.

The time series of disk-integrated radiances for the first 27 lunar calibrations (spanning 798 days from 14 November 1997 through 21 January 2000) are plotted in Fig. 1. The radiances in each band have been normalized by the value at the first calibration to show the relative changes in the instrument response as functions of time. Much of the variation in these time series is due to the changing observing geometry of the individual calibrations. Normalization of the calibration data for the observing geometry will be discussed in the next section.

3.3 NORMALIZING FACTORS

Although the surface of the moon remains unchanged over the lifetime of SeaWiFS, the radiance from the moon varies with the geometry of the observations. As a result, the disk-integrated lunar radiances are normalized to a common viewing geometry for incorporation into a lunar calibration time series. These normalizing factors are based, in large part, on the positions of the spacecraft, Earth, sun, and moon computed by the SeaWiFS navigation algorithms. The observing geometries for the lunar calibrations considered in this analysis are provided in Table 1. Using these values, five normalizing factors are calculated. These normalizing factors are discussed in detail in Barnes et al. (1998 and 1999). The implementation of these normalizing factors is discussed here.

The first normalizing factor corrects to a common sun–moon distance and varies as $1/R^2$, where R is the distance between two bodies. The sun–moon distance (D_{SM}) is normalized to 1 Astronomical Unit ($1\,\mathrm{AU} = 149.59787066 \times 10^6\,\mathrm{km}$):

$$N_1 \;=\; \left(\frac{D_{\mathrm{SM}}}{\mathrm{AU}}\right)^2. \tag{2}$$

The second normalizing factor corrects to a common SeaWiFS–moon distance and varies as $1/R^2$. The SeaWiFS–moon distance (D_{IM}) is normalized to the mean radius of the lunar orbit ($\mathrm{R_M}$= 384401 km):

$$N_2 \;=\; \left(\frac{D_{\mathrm{IM}}}{\mathrm{R_M}}\right)^2. \tag{3}$$

The third normalizing factor is the illuminated fraction of the lunar surface as a function of phase angle. This factor is a linear function of the phase angle, with the lunar surface fully illuminated at 0° phase, half illuminated at 90° phase, and dark at 180° phase. This function is given as:

$$f_1(\theta) \;=\; a_0 \;+\; a_1\theta, \tag{4}$$

where $a_0 = 1.0$ and $a_1 = -1/180$. Because the nominal phase angle of the lunar calibrations is 7°, the illuminated area of the lunar surface is normalized to the illuminated area at 7°:

$$N_3 \;=\; \frac{f_1(7^\circ)}{f_1(\theta)} \;=\; \frac{173.0^\circ}{180.0^\circ \;-\; \theta}, \tag{5}$$

The fourth normalizing factor compensates for the oversampling of the lunar image during the calibration. As discussed previously, the oversampling is a function of the pitch rate and the apparent size of the moon. Because the spacecraft does not have the use of its horizon sensors during the lunar pitch maneuver, there is increased noise in the pitch rate calculated from the attitude control system during the maneuver. As a result, the pitch rate is determined from the number of scan lines in the lunar image. The number of scan lines is computed from the maximum extent between the points whose brightness is 1% of the peak brightness in the image. For a given calibration, these distances are averaged over the eight bands. Because the number of scan lines in the lunar calibrations range from 23–29, these numbers are normalized to a common value of 25 scan lines. To compensate for the variation in the apparent size of the moon in the images, the number of scan lines is normalized to a common SeaWiFS–moon distance of the mean radius of the lunar orbit. The resulting normalizing factor is:

$$N_4 \;=\; \frac{25.0/N_{\mathrm{M}}}{D_{\mathrm{IM}}/\mathrm{R_M}}, \tag{6}$$

where N_{M} is the mean number of scan lines in the lunar image.

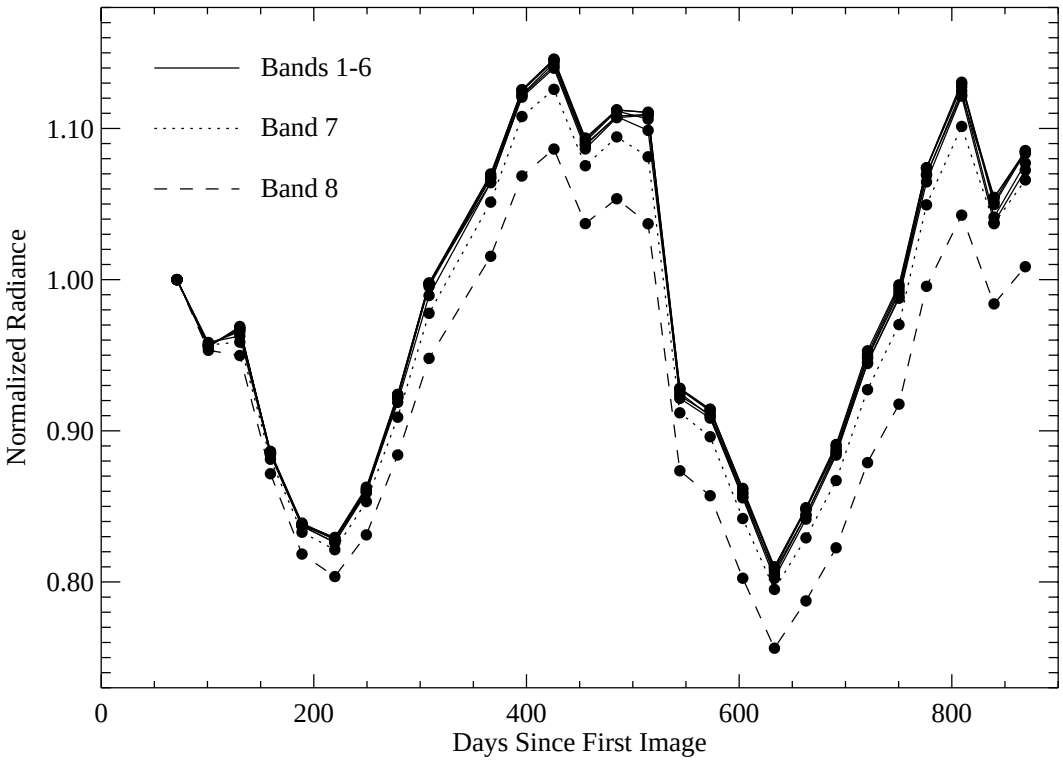

Fig. 1. Disk-integrated lunar radiances, normalized to the first calibration.

Table 1. Lunar calibration observing geometry. The notation [A] indicates the calibration was after zero phase; [B] indicates before zero phase. The symbol Δt_0 is the time (in days) since the first image.

Calibration	*Year*	*Date*	Δt_0	$D_{\rm SM}$ [AU]	$D_{\rm IM}(\rm R_M)$	θ [degrees]	$N_{\rm M}$
1	1997	14 Nov [A]	71.26	0.991602	0.939681	6.75	25.63
2		14 Dec [A]	100.83	0.986812	0.967318	7.03	25.35
3	1998	13 Jan [A]	130.39	0.986119	0.996159	5.45	24.57
4		10 Feb [B]	159.19	0.989545	1.01474	6.65	24.29
5		12 Mar [B]	188.89	0.996419	1.03299	6.72	23.62
6		12 Apr [A]	219.75	1.00516	1.03719	6.66	24.14
7		11 May [B]	249.38	1.01283	1.02474	7.10	25.75
8		10 Jun [A]	278.87	1.01790	1.00304	6.43	26.19
9		10 Jul [A]	308.36	1.01919	0.975564	5.70	26.69
10		5 Sep [B]	366.31	1.01050	0.932589	6.52	27.81
11		5 Oct [B]	395.73	1.00238	0.915500	6.69	28.47
12		4 Nov [A]	425.84	0.994060	0.910064	6.55	28.16
13		4 Dec [A]	455.33	0.988037	0.920501	7.03	27.24
14	1999	2 Jan [A]	484.89	0.985745	0.942602	6.73	28.29
15		1 Feb [A]	514.38	0.987825	0.970323	4.88	26.79
16		2 Mar [A]	544.20	0.993771	1.00182	7.38	26.34
17		31 Mar [B]	572.73	1.00158	1.01719	7.01	25.65
18		1 May [A]	603.38	1.01015	1.03724	6.92	25.62
19		30 May [A]	633.21	1.01647	1.03694	7.95	25.46
20		29 Jun [A]	662.83	1.01928	1.02351	7.25	25.94
21		27 Jul [B]	691.21	1.01814	1.01103	6.82	26.15
22		26 Aug [B]	720.76	1.01317	0.984094	6.72	26.81
23		25 Sep [B]	750.32	1.00553	0.954810	6.83	26.78

Table 1. (cont.) Lunar calibration observing geometry. The notation [A] indicates the calibration was after zero phase; [B] indicates before zero phase. The symbol Δt_0 is the time (in days) since the first image.

Calibration	*Year*	*Date*	Δt_0	$D_{\rm SM}$ [AU]	$D_{\rm IM}(\rm R_M)$	θ [degrees]	$N_{\rm M}$
24	1999	24 Oct [B]	776.21	0.997086	0.929820	7.25	27.78
25	1999	22 Nov [B]	809.28	0.989973	0.913459	6.66	27.78
26	1999	23 Dec [A]	839.72	0.985987	0.912118	9.83	28.80
24	1999	24 Oct [B]	776.21	0.997086	0.929820	7.25	27.78
25	1999	22 Nov [B]	809.28	0.989973	0.913459	6.66	27.78
26	1999	23 Dec [A]	839.72	0.985987	0.912118	9.83	28.80
27	2000	21 Jan [A]	869.13	0.986489	0.924960	8.61	29.02

The fifth normalizing factor corrects for changes in the brightness or reflectance of the moon with phase angle. The moon has a non-uniform particulate surface with large scale regional variations in reflectance. The nonlambertian change in the overall reflectance of the lunar surface with phase angle can be approximated by Hapke's bidirectional reflectance equation (Hapke 1986). Helfenstien and Veverka (1987) used Hapke's equation and a set of six empirically-derived constants, to provide a curve of disk-integrated reflectance versus phase angle for the moon. This curve is plotted in Fig. 2. A quadratic function has been fit to this curve to provide an interpolation between the data points. This interpolation scheme is limited to phase angles between 4° and 10°, using the function:

$$f_2(\theta) \;=\; b_0 \;+\; b_1\theta \;+\; b_2\theta^2, \qquad (7)$$

where $b_0 = 1.2872531 \times 10^{-1}$, $b_1 = -6.7007694 \times 10^{-3}$, and $b_2 = 2.1625472 \times 10^{-4}$. The normalizing factor is computed relative to the value at 7°, the nominal phase angle of the lunar calibrations:

$$N_5 \;=\; \frac{f_2(7^\circ)}{f_2(\theta)} \;=\; \frac{0.092414408}{b_0 \;+\; b_1\theta \;+\; b_2\theta^2}, \qquad (8)$$

The SeaWiFS lunar calibrations to date have occurred at phase angles of 4.8–9.8°, so the normalizing factor has been applied over a narrow range of phase. There are indications that the variation in lunar reflectance with phase angle has a wavelength dependence, which will be discussed in subsequent sections. There is also evidence that the moon is brighter before full phase than after (Kieffer and Anderson 1998). If this evidence is borne out, the brightness asymmetry would have an effect of 0.5–1.0% on the value of N_5. Approximately 40% of the lunar measurements to date were made before full phase.

The overall normalizing factor for each lunar measurement is the product of the five individual factors. This multiplicative factor is applied to the disk-integrated lunar radiances for each of the eight SeaWiFS bands. For the lunar calibrations to date, the value of the overall normalization factor has ranged from 0.783–1.10, with a mean value of 0.924. The time series of radiances normalized to the common viewing geometry are plotted in Fig. 3.

The phase angle is the most important of the geometric angular parameters for SeaWiFS lunar measurements. The variation of the integrated lunar radiance with phase angle is much stronger than any variation with libration angle. For libration changes, the loss of visible lunar surface from one side of the moon is balanced by the gain of visible surface on the other side. For disk-integrated spectral radiances over the course of several months to several years, libration is not expected to have a major effect on the slope of the time series, but is expected to increase the scatter in the data. The overall contribution of libration to the SeaWiFS lunar time series remains unknown and is not corrected in this analysis.

3.4 PHASE ANGLE CORRECTIONS

Two trends are apparent in the plots shown in Fig. 3. The first is a systematic variation in the data from one calibration to the next that probably arises from an incomplete normalization to a common viewing geometry rather than from instrumental effects. The fact that the data for bands 1–6 track each other supports this reasoning. The second trend is a decrease in the radiometric response of bands 7 and 8 with time.

The time series can be corrected for the incomplete normalization over viewing geomety by a second normalization based on a subset of the SeaWiFS bands. Barnes et al. (1998) based this second normalization on the values for band 5, while Barnes et al. (1999) based the normalization on the average of the values for bands 1–6. After 23 lunar calibrations, however, the consistency among these bands is less than it was for the data sets in Barnes et al. (1999). Barnes and McClain (1999) show that bands 3 and 4 appear to be changing the least among these bands, so the mean value of these bands at each calibration is used as the second normalization of the calibration time series. The radiances, with the second normalization applied, are plotted in Fig. 4. Identical results are obtained if the disk-integrated radiances are normalized to the first observation in each band and to the mean for bands 3 and 4 for each calibration. Examining Fig. 4 shows that the radiometric responses for bands 1–6 have changed slightly over the course of the mission, while the response for band

7 is down approximately 2.5% and the response for band 8 is down approximately 8%. It should be noted that calibrations 3, 9, and 15 occurred at phase angles of less than 6° and that calibrations 19, 26, and 27 occurred at phase angles of 8° or more.

The change in lunar reflectance with phase angle from Helfenstein and Veverka (1987) is monochromatic. The measurements used as a basis for their lunar reflectance model were made at wavelengths from 360–1,060 nm (Lane and Irvine 1973). Helfenstein and Veverka (1987) used the average of those measurements (over wavelength) to create a single, best-fit lunar reflectance curve at an undefined wavelength, presumably near 500 nm. The deviations of the low and high phase angle calibrations shown in Fig. 4 appear to vary in magnitude as a function of wavelength, indicating that wavelength-dependent phase angle effects are still present in the data. Barnes and McClain (1999) derived an empirical wavelength-dependent phase angle correction from the lunar calibration data that minimizes these deviations. Barnes and McClain (1999) only use the data points for calibrations 3, 9, and 15 to compute the corrections, while the implementation described here uses all 27 calibrations to compute the corrections.

The method for calculating the correction is as follows. For each band, a regression line is calculated from the normalized calibration data to determine the change in the output of the band with time. The low and high phase angle points are excluded from the calculations. Two piecewise fits are computed for each of bands 1–6: one quadratic and one linear. Three piecewise fits are computed for bands 7 and 8: two quadratic and one linear. For each band, the fractional differences between the measured calibration data points and the computed trend lines are computed as functions of the phase angles of the measurements:

$$f_3(\lambda,\theta) \;=\; \frac{L_m(\lambda,\theta) \;-\; L_c(\lambda,\theta)}{L_c(\lambda,\theta)}, \qquad (9)$$

where L_m is the measured radiance and L_c is the computed radiance. These differences are plotted in Fig. 5, along with linear fits to the differences. The slopes of these fits, $c_1(\lambda)$, are the wavelength-dependent phase angle correction factors. Examination of the plots in Fig. 5 shows there is a correlation between the differences and the phase angles over the entire range of phase angles. This is the reason that the implementation of the wavelength-dependent phase angle correction uses all 27 calibrations in computing the correction factors.

The normalizing factors for the lunar data are computed relative to the nominal phase angle of 7°:

$$N_6 \;=\; \Big(1.0 \;-\; c_1(\lambda)(\theta \;-\; 7.0^\circ)\Big). \qquad (10)$$

The correction factors for each band are given in Table 2. Values of N_6 are typically in the range of 0.987–1.010 for the observations. Because these correction factors are wavelength-dependent, these effects cannot be removed from the calibration data by the normalization to the mean of bands 3 and 4.

Table 2. Wavelength-dependent phase angle correction factors.

Band No.	λ [nm]	*Correction Factor* c_1 $(1/\theta)$
1	412	−0.0015091569
2	443	−0.0011531493
3	490	−0.00011397443
4	510	0.00011441961
5	555	0.0016632741
6	670	0.0033899319
7	765	0.0041000855
8	865	0.0044748836

N_6 is the final normalization applied to the lunar calibration data as part of the series of normalizations discussed in Sect. 3. The lunar data, with this correction applied, is then normalized by the mean values for bands 3 and 4. The resulting time series are plotted in Fig. 6. Comparing Fig. 6 with Fig. 4 shows that the wavelength-dependent phase angle correction reduces the scatter in the time series considerably. The time series for bands 1–6, with an expanded vertical scale, are plotted in Fig. 7.

3.5 LUNAR TIME CORRECTIONS

The CVT has used the lunar calibration time series shown in Fig. 6 and Fig. 7 to compute time correction factors for bands 1, 2, 5, 6, 7, and 8. The group used linear and quadratic fits to the lunar measurements to compute the changes in response of those bands with time. There is no lunar calibration information prior to the first lunar calibration, which was obtained on the 71st day after the first on-orbit SeaWiFS image was obtained. Consequently, the data for each band were renormalized from the plots in Fig. 6 and Fig. 7 so that the intercepts of the fits have values of unity at the time of the first image. The fits were sampled at the time of the solar calibrations to facilitate comparison of the lunar and solar calibration data.

The renormalized calibration time series for bands 1–6 are plotted in Fig. 8. For each of these bands, a single linear fit yields the best estimate of the change in response of the band with time. These fits are also plotted in Fig. 8. Bands 3 and 4 do not show any change in response over the course of the mission. The responses of the other bands are down: band 1 is down by 0.9%, band 2 is down by 0.5%, band 5 is down by 0.3%, and band 6 is down by 0.8%. Even though these changes are small, they could produce noticeable effects in the water-leaving radiances retrieved from the SeaWiFS ocean data, particularly for bands 1 and 6.

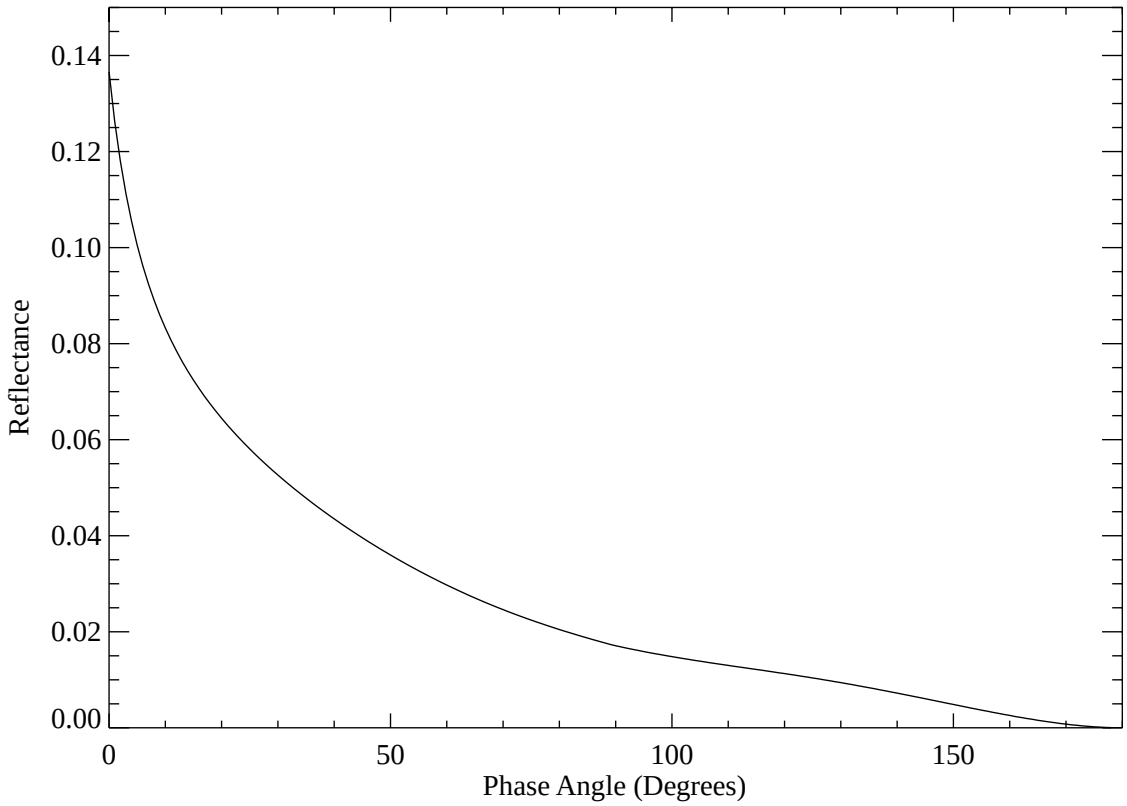

Fig. 2. Disk-integrated reflectances versus phase angle.

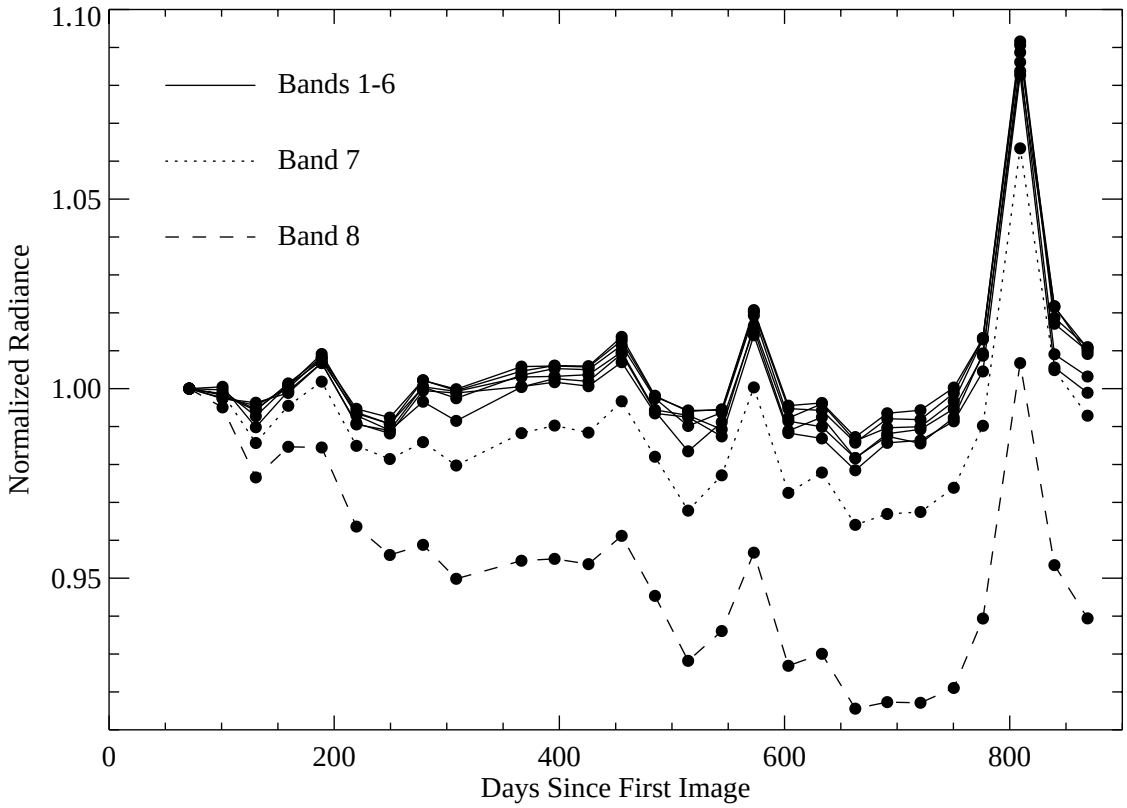

Fig. 3. Disk-integrated lunar radiances, normalized to a common viewing geometry.

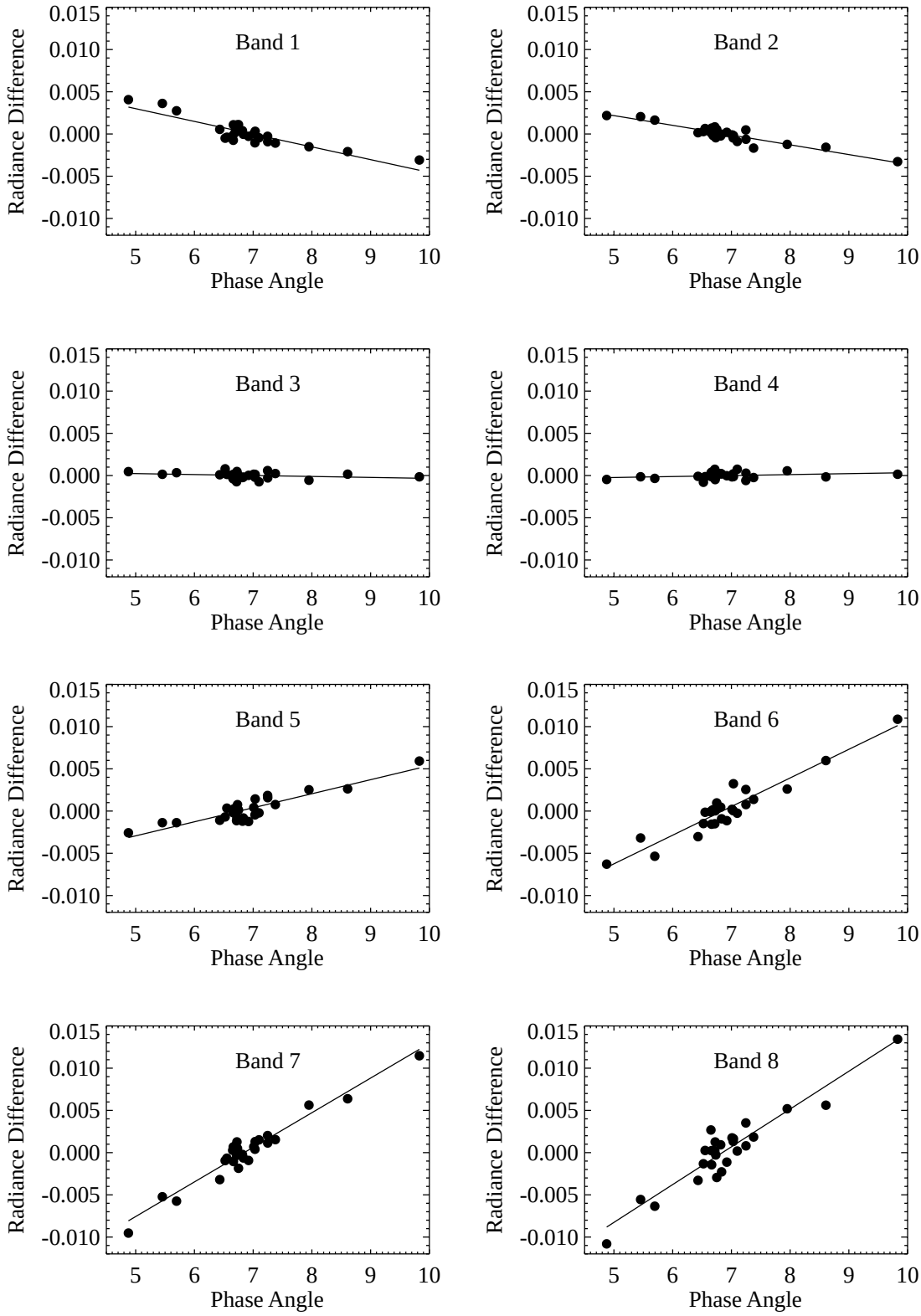

Fig. 5. Differences in measured and computed disk-integrated lunar radiances.

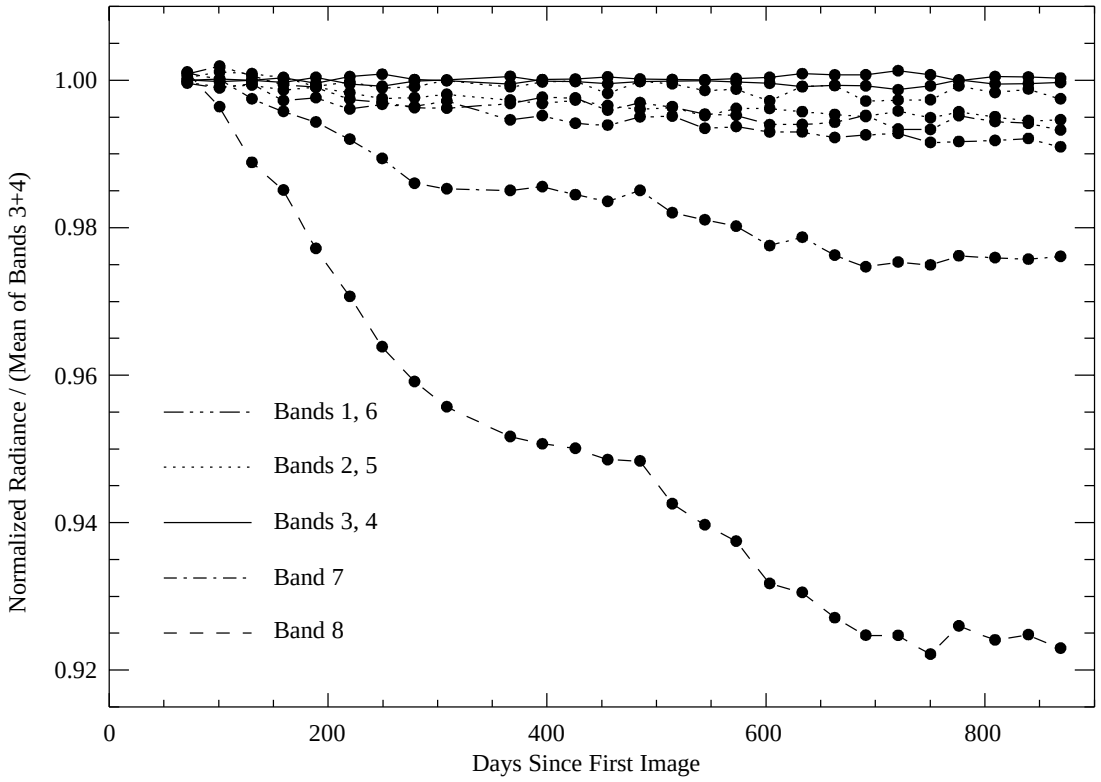

Fig. 6. Lunar calibration time series for bands 1–8.

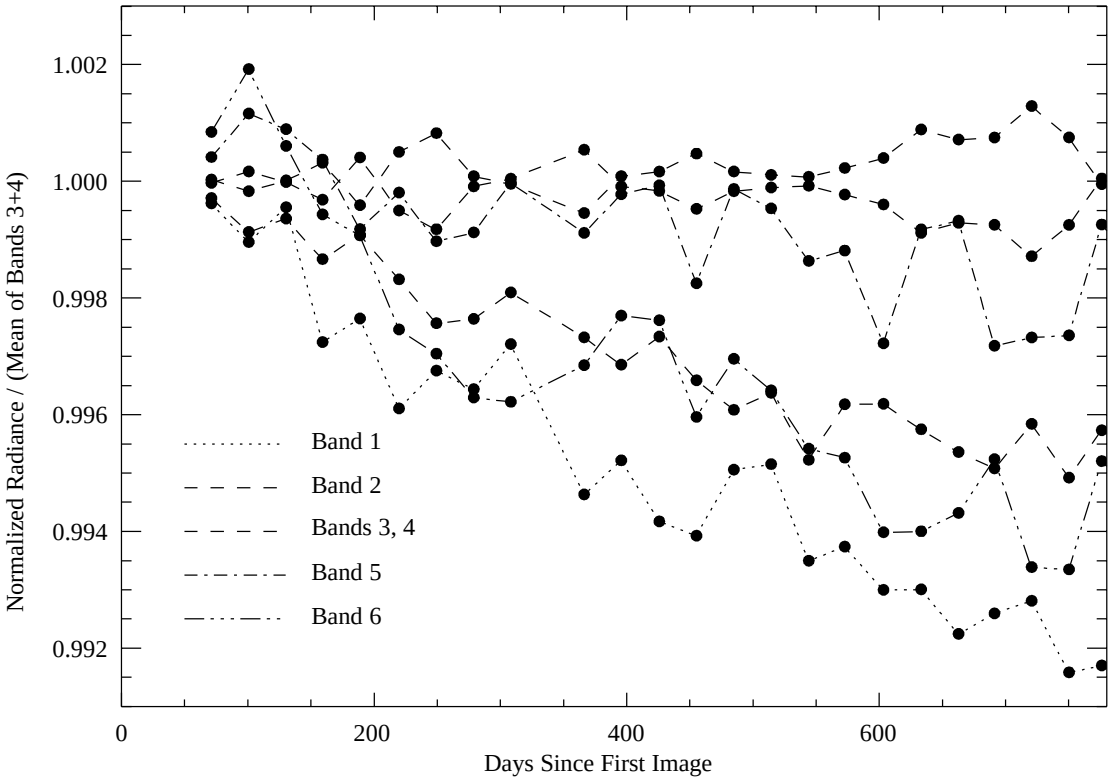

Fig. 7. Lunar calibration time series for bands 1–6.

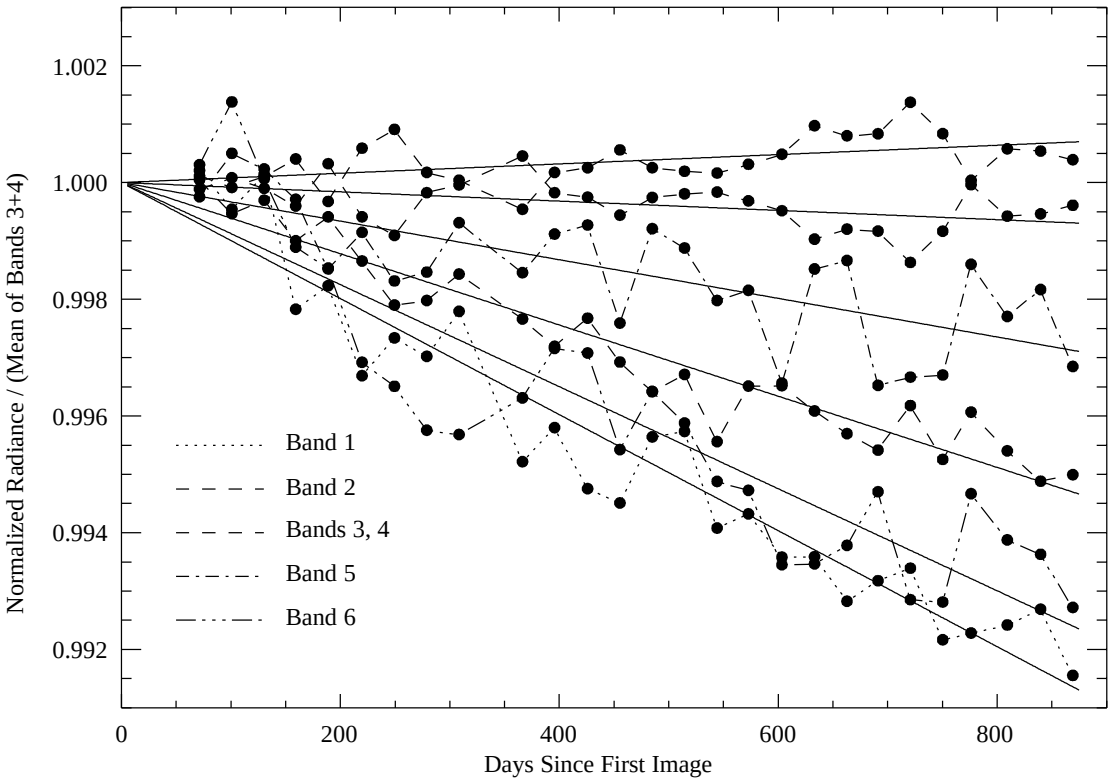

Fig. 8. Lunar calibration time series with linear fits for bands 1–6.

The renormalized calibration time series for all 8 bands are plotted in Fig. 9. The changes in response of bands 7 and 8 can be estimated by fits of two piecewise quadratic functions and one piecewise linear function. These functions are also plotted in Fig. 9. This figure also shows the linear fits for bands 1–6. Examining Fig. 9 shows that the change in response for bands 7 and 8 is 3.4% and 9.9%, respectively, over the course of the mission.

The time correction factors for bands 1, 2, 5, 6, 7, and 8 are computed from the inverses of the fits for these bands. There is a single correction for bands 1, 2, 5, and 6 and three piecewise corrections for bands 7 and 8. The single linear corrections for bands 1, 2, 5, and 6 and the piecewise linear correction for bands 7 and 8 are used to extrapolate the time corrections for these bands in time beyond the date of the last lunar calibration. These time correction factors provide a stable radiometric response for each of the SeaWiFS bands over the course of the mission. These factors are incorporated into the SeaWiFS calibration table, which is updated as required by the on-orbit performance of the instrument.

3.6 DISCUSSION

The CVT is continuing to investigate possible causes of the change in response of the SeaWiFS bands with time. A comparison of the lunar calibration data with the solar calibration data shows that the changes in response of bands 7 and 8 appears in both the lunar and solar data sets. Figure 10 shows the ratio of band 7 to band 8 computed from the solar measurements, as derived by Eplee et al. (2000), superimposed on the ratio computed from the lunar measurements plotted in Fig. 9. The solar ratio was normalized to have the same value as the lunar ratio on day 71—the day of the first lunar calibration.

The ratio of the functions fitted to the bands 7 and 8 lunar data is also plotted in Fig. 10. The plots show that the lunar and solar data are consistent and that the piecewise functions fitted to the lunar data are consistent with the observations. The deviation of the solar ratio from the lunar ratio prior to the first lunar calibration is caused by changes that occurred in the reflectance of the solar diffuser early in the mission (Eplee et al. 2000). The agreement between the lunar band 7:8 ratio and the solar band 7:8 ratio shows that the changes in response for bands 7 and 8 arise from changes in the instrument itself, and not from artifacts in either the lunar or solar data analyses.

One scenario for the changes in response of bands 7 and 8 is as follows. The long wavelength limit for the quantum efficiency of silicon photodiodes is about 1 m. At these wavelengths, near infrared photons penetrate the surface of the material to the point that the response of the diode to short-term changes in radiant flux is compromised. It is generally believed that, over extended periods of exposure, these long wavelength photons can also cause a degradation of the diode material. Engineers at the Santa Barbara Research Center, the manufacturer of SeaWiFS, call this process "annealing." The smaller change in response for

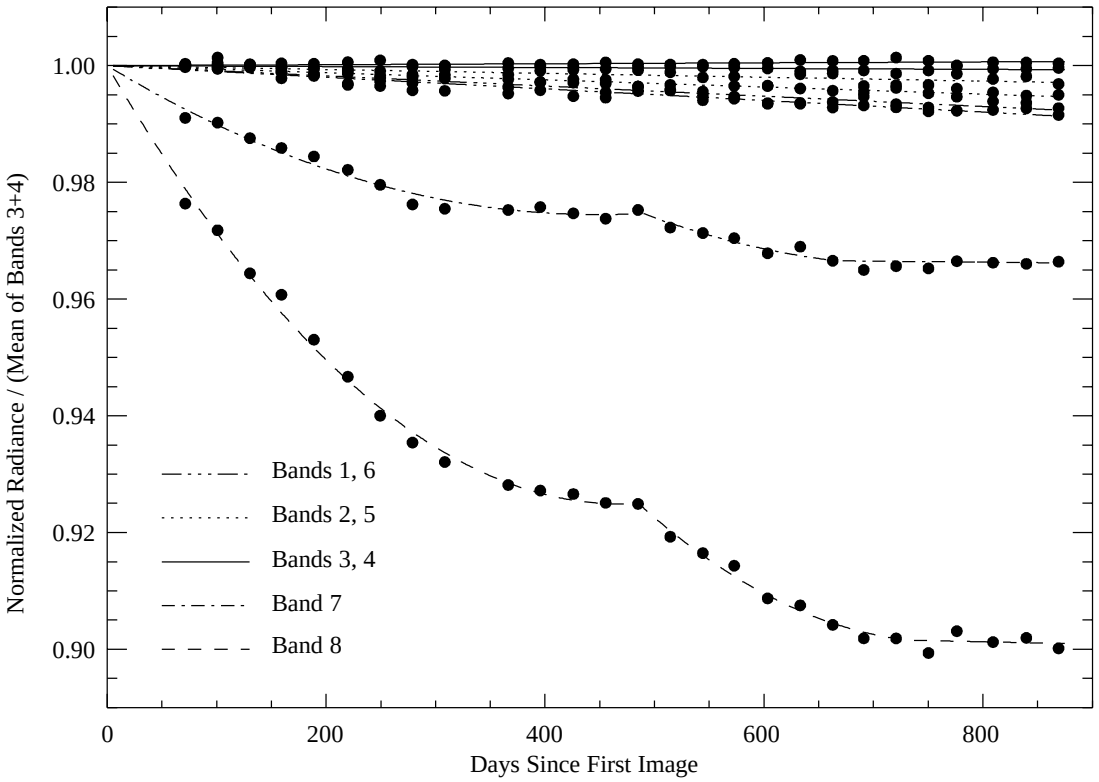

Fig. 9. Lunar calibration time series with linear fits for bands 1–8.

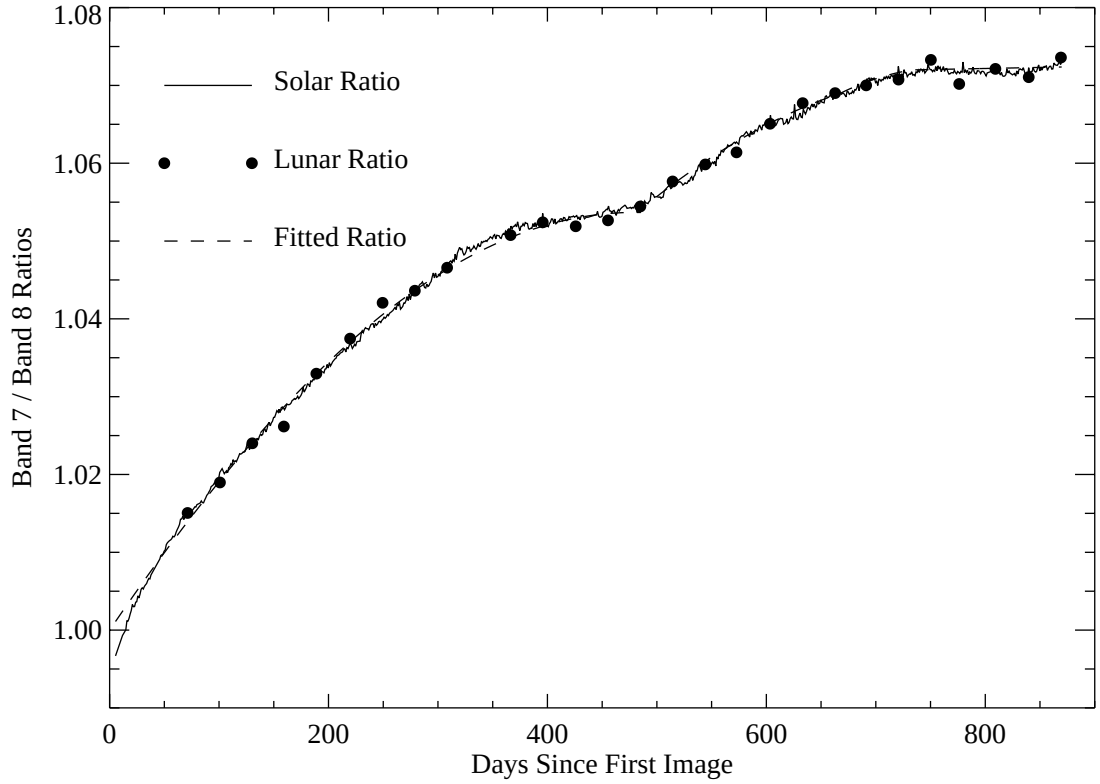

Fig. 10. Lunar and solar calibration band ratios for bands 7 and 8.

bands 5 and 6 may be due to the same process, just at shorter wavelengths.

The changes in the response of bands 1 and 2 require another scenario. Eplee et al. (2000) show that the reflectance of the SeaWiFS solar diffuser is decreasing with time, presumably due to photolyzed organic materials (outgassed from the spacecraft) condensing onto the surface of the diffuser. These materials preferentially absorb sunlight at shorter wavelengths, so the degradation of the diffuser reflectance decreases with increasing wavelength. Such yellowing of the diffuser was expected, based on experience with the Coastal Zone Color Scanner (CZCS). The SeaWiFS primary mirror is located behind an aperture in its rotating telescope housing, so it is not exposed to space in the manner of the solar diffuser. It is possible that the effects of the yellowing of the primary mirror are just now becoming observable.

REFERENCES

Barnes, R.A., R.E. Eplee, Jr., and F.S. Patt, 1998: "SeaWiFS measurements of the moon." In: Sensors, Systems, and Next-Generation Satellites II, *SPIE,* **3498,** 311–324.

Barnes, R.A., R.E. Eplee, Jr., F.S. Patt, and C.R. McClain, 1999: Changes in the radiometric sensitivity of SeaWiFS. *Appl. Opt.,* **38,** 4,649–4,664.

Barnes, R.A., and C.R. McClain, 1999: The calibration of SeaWiFS after two years on orbit. In: Sensors, Systems, and Next-Generation Satellites V, *SPIE,* **3870,** (in press).

Eplee, R.E., Jr., R.A. Barnes, and F.S. Patt, 2000: Solar data analysis for SeaWiFS calibration. ???This volume???

Hapke, B. 1986: Bidirectional reflectance spectroscopy. 4. Extinction and the opposition effect. *Icarus,* **67,** 246–280.

Helfenstein, P., and J. Veverka, 1987: Photometric properties of lunar terrains derived from Hapke's equation. *Icarus,* **72,** 342–357.

Johnson, B.C., E.E. Early, R.E. Eplee, Jr., R.A. Barnes, and R.T. Caffrey, 1999: The 1997 Prelaunch Radiometric Calibration of SeaWiFS. *NASA Tech. Memo. 1999–206892, Vol. 4,* S.B. Hooker and E.R. Firestone, Eds., NASA Goddard Space Flight Center, Greenbelt, Maryland, 51 pp.

Kieffer, H.H., and J.M. Anderson, 1998: Use of the moon for spacecraft calibration over 350–2500 nm. In: Sensors, Systems, and Next-Generation Satellites II, *SPIE,* **3498,** 325–336.

Lane, A.P., and W.M. Irvine, 1973: Monochromatic phase curves and albedos for the lunar disk. *Astron. J.,* **78,** 267–277.

Woodward, R.H., R.A. Barnes, C.R. McClain, W.E. Esaias, W.L. Barnes, and A.T. Mecherikunnel, 1993: Modeling of the SeaWiFS Solar and Lunar Observations. *NASA Tech. Memo. 104566, Vol. 10,* S.B. Hooker and E.R. Firestone, Eds., NASA Goddard Space Flight Center, Greenbelt, Maryland, 26 pp.

Symbols

a_0 Constant term of function of illuminated fraction of the lunar surface.
a_1 Linear term of function of illuminated fraction of the lunar surface.

b_0 Constant term of interpolation of lunar phase function.
b_1 Linear term of interpolation of lunar phase function.
b_2 Quadratic term of interpolation of lunar phase function.

C_{dark} Dark count from sensor output data.
C_{out} Counts from sensor output data.
c_1 Wavelength-dependent phase angle correction factors.

D_{IM} SeaWiFS–moon distance in the mean radius of the lunar orbit (R_{M}).
D_{SM} Sun–moon distance in astronomical units (AU).
d Detector.

f_1 Illuminated fraction of the lunar surface.
f_2 Interpolated lunar phase function.
f_3 Difference between measured and fitted integrated lunar radiances.
g Gain.

K_1 Counts to radiance conversion factor.
K_2 Detector temperature-dependent correction factor.
K_3 Scan modulation correction.

L_c Fitted integrated lunar radiance.
L_m Measured integrated lunar radiance.
L_S Calibrated at-sensor radiance.

M Half-angle mirror side correction factor.
ms Half-angle mirror side.

N_{M} Mean number of scan lines in a lunar image.
N_1 Lunar radiance normalizing factor to a common sun–moon distance.
N_2 Lunar radiance normalizing factor to a common SeaWiFS–moon distance.
N_3 Lunar radiance normalizing factor for the illuminated fraction of the lunar surface.
N_4 Lunar radiance normalizing factor to a common number of scan lines in a lunar image.
N_5 Lunar radiance normalizing factor to a common phase angle.
N_6 Lunar radiance normalizing factor for the wavelength-dependent phase angle correction.

pxl Pixel number along a SeaWiFS scan line.

R Distance between two bodies.
R_{M} Mean radius of the lunar orbit.

T Detector temperature from the sensor output data.

t Time tag of the sensor output data.

t_0 Reference time for temporal corrections to the radiometric response of the instrument.

T_{ref} Detector reference temperature.

α SeaWiFS vicarious gain.

β Constant term in the temporal correction to the radiomteric response of the instrument.

γ Linear term in the temporal correction to the radiometric response of the instrument.

δ Quadratic term in the temporal correction to the radiometric response of the instrument.

θ Phase angle of the luanr calibrations.

λ Wavelength.